Standardizing designed and emergent quantitative features in microphysiological systems

Nahon, D.M.; Moerkens, R.; Aydogmus, H.; Lendemeijer, B.; Martinez-Silgado, A.; Stein, J.M.; ... ; Mummery, C.L.

nature biomedical engineering

Supplementary information

https://doi.org/10.1038/s41551-024-01236-0

Standardizing designed and emergent quantitative features in microphysiological systems

In the format provided by the authors and unedited

Contents

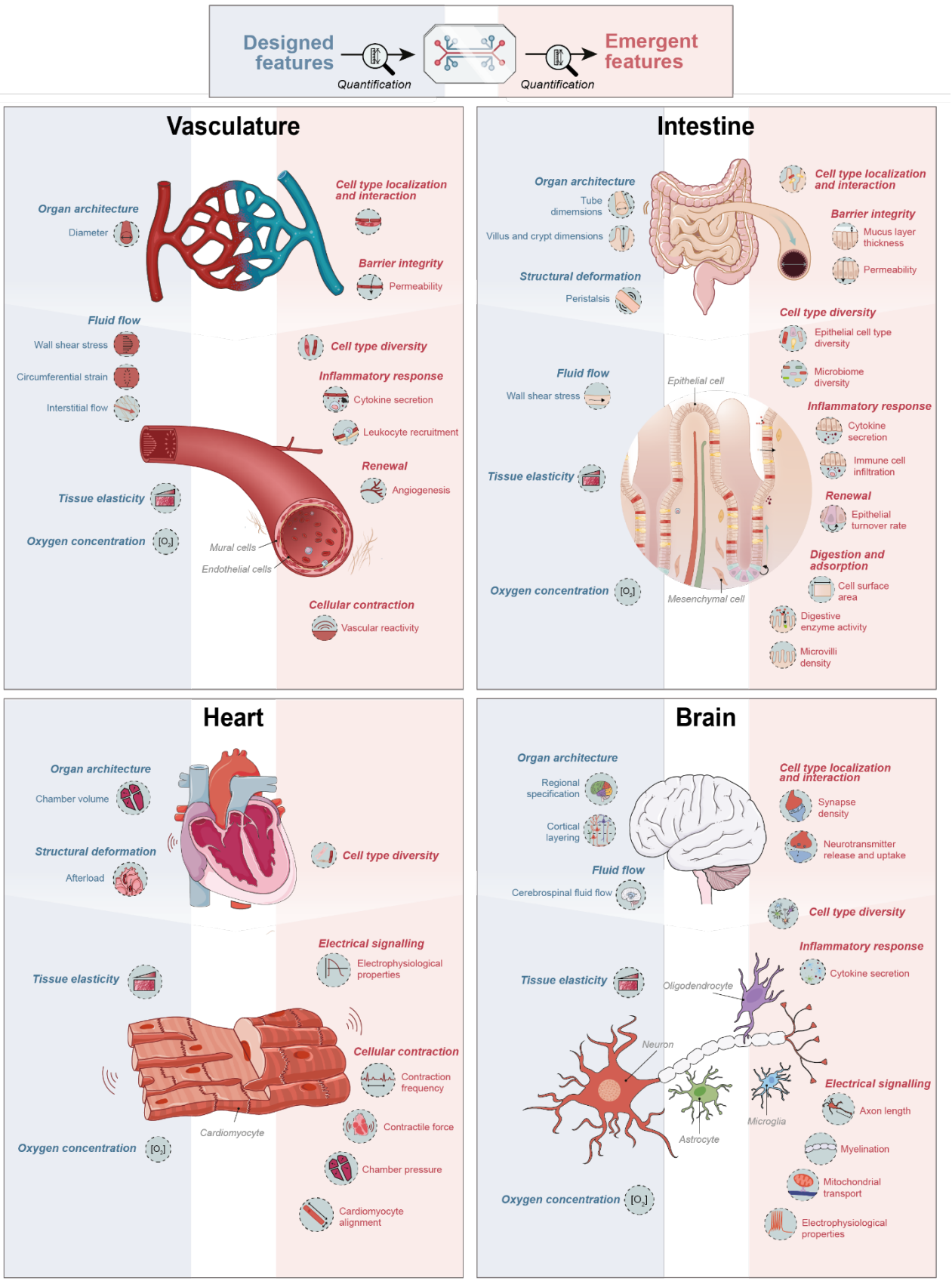

Supplementary Fig. 1 | Schematic overview of physiological features of the human vasculature, intestine, heart and brain. Physiological features can be divided into 'designed' (blue) and 'emergent' (red). Features may belong to either or both groups depending on the specific model and functional read-out required. Detailed descriptions of organ physiology and these features are provided in Supplementary Discussion 2.

Supplementary Table 1 | Quantification of organ-specific designed and emergent physiological features in microphysiological systems and in humans.

Category	Organ	Feature	MPS, method	MPS, quantification	Human, quantification	MPS, Ref.	Human, Ref.
Fluid flow	Vessel	Interstitial flow	Pressure pump	1.3 µm/s	0.1-2 µm/s (rabbit)	1	2
Cell-type diversity	Intestine	Microbiome – bacterial diversity	CFU count; 16S rRNA sequencing	118-135 OTUs (primary cells, Ileum) and 200 OTUs (Caco-2)	280 OTUs	3	4
Inflammatory responses	Vessel	Patrolling monocyte speed	Real-time fluorescent imaging	3-12 µm/min	9-36 µm/min (mouse)	5	6
	Intestine	Immune cell infiltration	IF	22-25 CD103+ cells /µm^2 in epithelial layer upon LPS stimulation	≤ 25 IELs / 100 epithelial cells (Duodenum, healthy)	7	8
Barrier integrity	Intestine	Mucus layer thickness	Dark field microscopy and beads	Outer layer: 370 µm, inner layer: 200 µm	SI: 50-450 µm; LI: outer layer 300-700 µm, inner layer 100-400 µm	9	10
Electrical signalling	Brain	Axon length	Compartmentalized system	9 - 12 cm	> 1 meter	11	12
		Myelin thickness	Electron microscopy on compartmentalized system	Average G-ratio of 0.57 ±0.16	G-ratio of 0.68-0.8	13	14
		Myelin length	IF and artificial 'axons'	10 - 120 µm	18.28-57.36 µm (mouse)	15	16
		Axonal transport speed of mitochondria	Directed axonal growth in compartmentalized system	0.6 µm/s	0.22 µm/s (mouse)	17	18
Cellular contraction	Heart	Contraction frequency	Video tracking	55-80 BPM	~64 BPM	19	20
			Video tracking	43-57 BPM		21	
			Pillar tracking	32 BPM		22	
		Contractile force	Pillar tracking	6.2 ± 0.8 mN/mm^2	44 mN/mm^2	23	24
			Pillar tracking	~12.5 µN		25	
			Pillar tracking	~3 mN/mm^2		26	
		Force-frequency relationship	Video tracking	Positive	Positive	25	27
		Cardiomyocyte alignment	Optical imaging	88-96/12.5-13.5 µm (Aspect ratio: 7.6±0.4:1)	141/19 µm (aspect ratio: 7.4:1)	23	28
		Systolic ventricular pressure	Intraventricular pressure sensor	50 µmHg	120 mmHg	29	30
Digestion and absorption	Intestine	Cell surface area	Imaging and computational 3D reconstructions	Enlargement factor (apical cell surface compared to monolayer): 1.7-fold (excluding microvilli)	Enlargement factor villi: 4.5-8.6 (SI). Enlargement factor microvilli: 9.2-15.7 (SI), 6.4-6.7 (LI)	31	32,33
		Microvilli density	SEM and ImageJ	7/µm^2	Jejunum: 114/µm^2 (Villus crest), 22/µm^2 (Intervillus space), 15/µm^2 (Crypt)	34	35
		Glucose uptake rate	Quantification of glucose in medium	~280 mmol L^{-1} h^{-1}, ~0.3 nmol cell^{-1} h^{-1}	Vmax= 83/25 mmol/h/15-cm segment and Km= 154/50 mmol/L (Jejunum/Ileum)	31	36
		Digestive enzyme activity	Aminopeptidase activity assay, A4N	9, 12 fmol/min/cell (flow, flow and strain)	—	37	
				0.92 fmol/min/cell		38	
			Sucrase-isomaltase activity assay (30 mM sucrose to glucose)	15-40 U/g protein	Vmax=83/36 mmol/h/15-cm segment and Km=142/74 mmol/L (Jejunum/Ileum)	39	36
		Drug metabolizing enzyme activity	LC-MS of metabolized drug in outflow (testosterone to 6β-OH-T)	0.056 nmol/min/mg protein	0.36-2.46 nmol/min/mg protein (Jejunum)	34	40

Data was included based on the criteria as stated in Supplementary Discussion 1 and quantified features are discussed in Supplementary Discussion 3 and 4. Abbreviations: — indicates that data are not available, MPS=microphysiological system, SI=small intestine, LI=large intestine, IEL=intraepithelial lymphocyte, CFU=colony-forming unit, OTU=operational taxonomic unit, LC-MS=liquid chromatography-mass spectrometry, IF=immunofluorescence, LPS=lipopolysaccharide, 6β-OH-T=6β-hydroxytestosterone, m=meter, BPM=beats per minute, N=Newton, h=hour, min=minute, s=second, ref=reference.

Supplementary Discussion 1 | Methodology

The current review is the outcome of the Netherlands Organ-on-Chip Initiative, a program with specific interest in developing advanced OoC systems for the vasculature, intestine, heart and brain. The decision to focus on the vasculature, intestine, heart and brain was developmentally driven: including derivatives of all three germlayers, an endodermal (intestine), ectodermal (brain) and mesodermal (heart) organ, with the vasculature as a link to all.

The review was based on the following stepwise approach:

1. Determine the specific physiological features of each organ of interest. Of note: for each selected organ, we discuss an extensive but not exhaustive list of physiological features that have been quantitatively modelled in MPS. In addition, for some features, the implications for a specific MPS can be extrapolated to other organs.
2. Identify literature describing MPS of each selected organ that meets the following criteria;
    - The model system falls within our MPS definition. A broad and inclusive definition of MPS was adopted, to capture all of those relevant for the four organs selected. Microdevices containing cells in 2D or 3D cultures that either replicate the mechanical microenvironment by integrating fluid flow or mechanical actuation, or that integrate sensing modalities. We included systems that employ direct cell culture inside microfluidic or actuating systems, as well as those that integrate pre-engineered 3D tissues in these systems. The majority of discussed systems are microfluidic systems, which we refer to as Organ-on-Chip (OoC). Exceptions to this definition are clearly indicated in the text with the reason of inclusion. We excluded organoid cultures, since their stochastic, self-organizing nature generally precludes controlled confinement, and systems that model organ-organ connections in light of our focus on organ-specific features.
    - Reports accurate quantification of one of the defined physiological features of an organ or tissue in a healthy state. We focused on quantification of a healthy organ or tissue as this provides a baseline for comparing aberrant organ functions in disease.
    - Human cells were used in the system (primary, immortalized or iPSC-derived). Exceptions in which uses animal cells in a MPS are clearly indicated in the text.

3. Extract quantitative MPS values from the papers
4. Determine the best example to highlight. Selection was based on the most accurate quantification method, comparability with *in vivo* observations, the most suitable MPS type or an example which highlights an important consideration regarding quantification of that specific physiological feature.
5. Search for and extract, whenever possible, *in vivo* quantification of the specific physiological feature in human tissue. If human observations *in vivo* were not available, we sometimes included animal data. The result of these steps can be seen in Table 1 and Supplementary Table 1.

Identify technical advances which could overcome limitations in the current quantification methods of each physiological feature. Applicable technologies for MPS were considered which could improve quantification by either increasing the accuracy of measurement or improving the *in vivo* comparability. The proposed advances were grouped into several overarching technological areas to enable a more general overview on MPS technology and its areas of potential improvement.

Supplementary Discussion 2 | Organ physiology and features of the human vasculature, intestine, heart and brain

Physiological features can be divided into 'designed' and 'emergent' (Supplementary Fig. 1). Features may belong to either or both groups depending on the specific model and functional read-out required. In this review, they are divided for simplicity into one of the categories depending on the context discussed in this review. Microphysiological systems (MPS) can quantitatively control and monitor physiological features. Accurate quantification of these features is essential for system-to-system comparisons and understanding in vivo relevance which will facilitate development of measurable standards to designate a system as 'fit for purpose'. Here, we describe the basic organ physiology and biological features for the human vasculature, intestine, heart and brain (Supplementary Fig. 1).

Vasculature. Blood vessels are cylindrical tubes with diverging diameters which transport oxygen and nutrients through the body and remove waste products. The vessel wall consists of a single layer of endothelial cells surrounded by either smooth muscle cells or pericytes, depending on tissue location. There is also broad molecular heterogeneity within the vascular bed depending on the position in the vascular tree and the microenvironment of the surrounding tissue. Vascular cells sense and respond to many biomechanical and biochemical cues. Hemodynamic forces such as wall shear stress and circumferential strain or exerted by interstitial flow, tissue elasticity and the local oxygen concentration are examples of such cues. Blood vessels can actively respond to these signals by contracting or dilating (vascular reactivity), forming new blood vessels from those pre-existing (angiogenesis), or adjusting barrier integrity between the blood and the surrounding tissue to transport cytokines, hormones and other plasma constituents. Among the most important functions of blood vessels is responding to inflammatory stimuli by secreting cytokines and enabling immune cell transmigration.

Intestine. The intestine digests and selectively transports nutrients from its lumen to the bloodstream (small intestine) and absorbs remaining water and salts (large intestine). The enormous absorption capacity is related to the specific organization of the epithelial lining into finger-like structures (villi) and crypts, which increase the effective surface area. Epithelial cells start as stem cells in the crypts, migrate along the villus while maturing into functional cells and reach the tip of the villus after 3-4 days, which marks the end of their life cycle. They are organized along the villi according to their function (e.g. production of digestive enzymes, hormones and mucus along the villus length; epithelial regeneration and production of anti-microbial peptides in the crypt). The uptake of nutrients and transport of waste is facilitated by the mechanical microenvironment: peristaltic motion caused by a layer of longitudinal and circular (smooth) muscle cells resulting in continuous flow of luminal content. The intestine is also an important barrier that actively controls the transport of luminal content to the circulatory system. The mucus layer forms the first mechanical barrier, followed by the tight epithelial layer that maintains barrier integrity and intestinal homeostasis. Immune cell surveillance of the epithelial barrier determines whether tolerance is maintained or inflammation elicited in response to digested and transported macromolecules. Oxygen gradients from the small- to the large intestine and from the lumen to the *lamina propria* allows survival of specific commensal microorganisms in each region without compromising the survival of adjacent intestinal epithelial cells. The commensal microorganisms that thrive in the anaerobic environment of the intestine are essential for both digestion and regulation of the intestinal immune response.

Heart. The heart pumps blood through the vasculature to distribute oxygen and nutrients and remove carbon dioxide and metabolic waste. It consists of four chambers (two upper atrial chambers and two lower ventricular chambers), which synchronously pump blood to either the lungs or rest of the body using valves to prevent blood backflow. It is made up of the contractile cardiomyocytes and multiple non-cardiomyocyte cell types such as fibroblasts, endothelial-, endocardial-, epicardial-, neuronal and immune cells. The sinoatrial node, which acts as the pacemaker, works in combination with the atrioventricular node and the Purkinje fibers to propagate electrical signals throughout the myocardial wall regulating cardiomyocyte contraction. The resulting contractile frequency and force are highly dependent on the cellular organization (e.g. coupling, alignment) of the cardiomyocytes and other cell types. Resident fibroblasts ensure the extracellular matrix (ECM) is well-maintained via protein turnover, thus controlling heart tissue elasticity. In the heart, varying (or reduced) oxygen concentrations are key in the onset or development of cardiac disease, as in myocardial infarction.

Brain. The human brain is organized in distinct functional and structural domains: the cerebrum, cerebellum and brainstem. Different brain regions, such as the hippocampus, cerebellum and the prefrontal cortex, have distinct topographical structures. Higher cognitive functioning is thought to arise from the prefrontal cortex, a

layered sheet of neural tissue with topographic separation into functional domains. Each brain region and neural cell type are distinct in their function and interaction, ensuring proper brain function. Besides blood flow, the brain is perfused by cerebrospinal fluid. This fluid is continuously produced by the choroid plexus and is involved in the distribution of nutrients and clearance of waste products. The brain is a highly active organ, so adequate oxygen levels are essential for maintaining proper brain function. At a cellular level, diverse neuronal subtypes and glial cells, such as astrocytes, microglia and oligodendrocytes, form neural networks that produce the brain output. Neurons communicate via these neural networks between- and within brain regions by propagating electrical signals (action potentials) along their axons, ultimately transmitting these through synapses using various neurotransmitters. This energy-consuming process requires mitochondrial anterograde transport along the axons for molecules and ions to reach the axon terminal, whereas retrograde transport is important for removing damaged organelles and debris. Astrocytes promote neuronal maturation and synapse development, maintain the blood-brain-barrier, provide neurons with metabolites and govern network activity. Oligodendrocytes produce an insulating layer, myelin, around the axons of neurons, ensuring efficient propagation of action potentials. The brain is a soft organ, more than 20% of this organ is made up of ECM, providing a scaffold for neural cells to migrate and make connections to other brain regions. Upon injury, microglia and astrocytes release and respond to inflammatory cytokines, creating scar tissue and removing debris from the extracellular space.

Supplementary Discussion 3 | Organ-specific designed feature
Quantifications presented in Supplementary Table 1

Fluid flow – interstitial flow
Interstitial flow describes the movement of fluid through the ECM and its resident cells and is the type of flow present in almost all tissues and organs. The forces exerted on cells by interstitial flow are more challenging to measure or calculate *in vivo* and *in vitro* and are therefore expressed as fluid flow speed. In the vasculature, interstitial flow has been described in great detail and it has been associated with vasculogenesis, lymphogenesis and lymphatic drainage of blood plasma which has leaked from the micro-vasculature. A similar process takes place in the brain, where cerebral spinal fluid (CSF), produced by cells of the choroid plexus, flows via the four ventricles of the brain to subarachnoid spaces, clearing waste products, distributing trophic factors and maintaining brain pH balance in the process[41]. OoCs have been able to model interstitial flow using 3D hydrogel compartments with known biophysical parameters suitable for convection of fluid at controllable velocities. In one technologically-advanced approach, a hydrogel containing a self-assembled vascular network was pressurized using a pump to apply constant interstitial flow[1]. Both computational simulation of flow velocities and verification using fluorescence recovery after photobleaching (FRAP) showed that interstitial flow was in the physiological range (Supplementary Table 1). Interestingly, the device design also allowed direct sampling of the interstitial fluid enabling investigation of therapeutic molecule distribution. This type of system is suitable for use on tissues embedded in a hydrogel; however, it cannot be applied to free floating tissues in culture. This is exemplified by a BoC system which uses rat cortical neurospheroids to study the effect of flow on waste clearance and neuronal maturation. Here, an osmotic micropump was used to apply a constant flow of 0.15 μl/min over spheroids trapped in concave microwells at the bottom of the microfluidic channel[42]. Improved neuronal differentiation and synapse formation was observed within the neurospheroid, suggesting that a rudimentary model of CSF flow can already benefit neuronal maturation. As described, there are multiple technological solutions to create intersitial flow. Important for correct quantitative implementation of these forces is the correct verification within the system. Multiple methods can be used to do so, including computational simulation and FRAP as previously discussed for VoCs[1].

Supplementary Discussion 4 | Organ-specific emergent feature
Quantifications presented in Supplementary Table 1

Cell type diversity – microorganisms
Non-human cells, such as commensal microorganisms in the intestine, can be quantified using another type of analysis: 16S rRNA sequencing. This technique was used to quantify microbiome diversity in a GoC system[3] (Supplementary Table 1). The healthy human microbiome is composed of ~200 species[43]. Modeling the microbiome *in vitro* thus requires a complex environment that supports many different species, with different needs in terms of oxygen concentration, nutrition and space. A GoC system containing over 200 unique operational taxonomic units (OTUs) from healthy human stool specimens was reportedly sustained for at least five days, comparing favorably with 280 OTUs in human intestinal aspirates[3]. Sequencing 16S rRNA is suitable to quantify microbial diversity in *in vitro* models, since the same methods can be used to characterize microbial diversity in intestinal brush border or stool samples. Alternatively, metagenomic sequencing provides insight in active microbial metabolic pathways and is applied to different areas of the human intestine to get insight into the contribution of location-specific microbiome niches.

Immune cell migration speed
Quantification of the number of transmigrated or infiltrated immune cells are clinically relevant proxies for the inflammatory and disease state[44]. The quantification of transmigrated or infiltrated immune cells requires normalization to the total tissue area analyzed[45,46]. This principle has been applied in both VoC and GoC systems. One VoC model quantified transmigration of neutrophils on a template-based vessel containing several cylindrical ECM-filled stacks with known volume[47]. Accordingly, the number of transmigrated neutrophils per tissue volume could be derived in a similar way as in mice. Also self-assembled 3D vascular networks have proven useful for investigating the dynamics of monocyte transmigration in real-time[48]. However, both models lack continuous perfusion and cannot be used to quantify flow-related parameters such as monocyte patrolling speed. This still requires more classical *in vitro* approaches; for example an endothelial cell monolayer under physiologically-relevant shear flow was used to quantify monocyte migration speed (3-12 μm/min); this was shown to be close to that in mice (Supplementary Table 1)[5,6]. To increase *in vivo* relevance further, future VoC models should include fluid flow and appropriate tissue elasticity. The importance of this was shown recently in work combining hydrostatic pressure driven flow over microfluidic channels in a collagen-based ECM[49]. The former VoC work can be extended by analysis of the migration of immune cells through an endothelial cell layer into a tissue, as was done in a GoC system. This multi-cell type systems contained a microchannel with an intestinal epithelial cell layer membrane-separated from a microchannel with an endothelial cell layer and monocyte-derived macrophages and dendritic cells. Using this system the number of dendritic cells invading the epithelial layer upon LPS stimulation was quantified to be ~22-25 $CD103^+$ cells/μm^2 of the epithelial layer[7]. Essentially the same method is used to study chronic inflammatory diseases. For example, to diagnose celiac disease, the number of invading inflammatory immune cells is measured in human intestinal biopsies. Of note, the units slightly differ making direct comparison difficult: for GoCs the number of immune cells/μm^2 of epithelial cell layer was reported, whilst for intestinal biopsies they reported the number of intraepithelial lymphocytes per 100 epithelial cells which circumvents the need to determine surface area (Supplementary Table 1). A similar unit can be used to express invading immune cells in GoCs. To date, the number of HoC models that incorporate components of the immune system are limited and robust quantifications on inflammatory response are lacking.

Barrier integrity – Mucus layer
Several GoC studies have quantified mucus production, either as dissociated mucin proteins in flow-through fluid[3,39] or as mucus layer thickness after fixation[31], which alters mucus layer structure. Dark-field microscopy is a non-invasive alternative allows study of the mucus layer in live cultures over time[9]. The outer and inner mucus layers can be distinguished based on pore size using fluorescently-labelled beads. Their thickness was estimated as 370 μm and 200 μm, respectively after 14 days in a GoC containing primary colon tissue. The chip design used required the removal of thin layers of PDMS parallel to the channels and subsequent analysis of the chips on a glass slide. Altering device design or advanced imaging methods might overcome this limitation (as discussed in the section 'Technical advances for the quantification of physiological features').

Electrical activity – Brain
Neurons in the brain show great diversity in axon length, extending away from the cell body, to establish connectivity within the brain and relay signals to the remainder of the body using motor neurons[12]. Modelling the extension of these long axons has been done using a compartmentalized microfluidic devices[11]. In these BoC devices, hiPSC-derived motor neurons grew as bundles of axon up to 9-12 cm in length. Whilst

remarkably long, the neurons were nevertheless approximately 100-fold shorter than *in vivo* equivalents. To relay signals throughout these elongated cells effectively, action potential conduction velocity needs to be ensured. For this, neurons require both myelination of their axons and active transport of mitochondria along these axons. Robust modelling and quantification of myelination and the build-up of small lipid-rich insulators, has only been described in a few MPS platforms. Among these is a nerve-on-chip device which described myelination of peripheral motor-neuron axons by Schwann cells, during guided outgrowth of axons from 3D spheroids[13]. Importantly, the model could be directly compared with *in vivo* measurements by using the same method and unit (Supplementary Table 1). Electron microscopy was used to quantify the G-ratio i.e. the ratio between the inner and the outer diameter of the myelin sheath as a measure of myelin thickness. The BoC value was slightly lower than the G-ratio described for the human central nervous system (Supplementary Table 1). This fits the notion that G-ratios in the peripheral nervous system are generally lower; however, these values have not been quantified *in vivo* to our knowledge. Another MPS of the brain was used to quantify myelin length in rat oligodendrocytes using immunofluorescent microscopy (Supplementary Table 1)[15]. Values were similar to the myelin length in mouse brain[16]. Active transport of mitochondria was measured in BoCs with microtunnel-separated culture compartments for the neuronal *soma* and thus forcing directed axonal outgrowth through the microtunnels and enabling live tracking of the mitochondria. This set-up allowed anterograde and retrograde transport of mitochondria to be distinguished with rates around 0.6 μm/s, the same order of magnitude as *in vivo*[17] (Supplementary Table 1).

Cellular contraction

Contraction is the functional output of muscle tissues. The heart relies on the synchronized and timely contraction of muscle cells to pump blood through the body. Alignment of contractile myocytes is essential in efficient unidirectional muscle contraction, therefore, it also serves as one output of *in vitro* maturity and increased physiological mimicry.

Alignment of muscle cells can be quantified using their aspect (length to width) ratio in the direction of contraction[50]. Aspect ratios can increase in response to the cardiomyocyte environment and mechanical or chemical signals[51–53]. For instance, in EHTs made in an oval cell culture chamber with standing pillars, cardiomyocyte alignment is induced by the chamber shape and subsequently by unidirectional load from the pillars. Aspect ratios of 7.6 ± 0.4 have been reported in EHTs which resembles that of healthy human adult myocardium [23] (Supplementary Table 1).

The overall output of the contraction of the cells can be described by its frequency, force and the force-frequency relationship (FFR). Cardiac muscle contraction frequency or rate is measured in beats per minute (BPM). This is easily quantified in MPS of the heart, for example by video tracking, but varies based on mechanical environment, cell-source and medium composition. Nevertheless, identifying factors affecting beat rate can provide insight into human physiology and facilitate drug discovery. For instance, beta-adrenergic signaling affects beating frequency[54]: in a cantilever-based cardiac model, seeded with hiPSC-derived cardiomyocytes in a constrained gel, baseline beat-rates were close to those in human heart and increased by ±60% upon beta-adrenergic stimulation (Supplementary Table 1). Importantly, many cardiac diseases or drug side effects manifest as arrythmias which can be detected by irregular beating.

Quantification of force is in most MPS of the heart only possible indirectly, optical displacement of cells being taken as a measure of contraction[55]. Other studies optically track anchoring points with known stiffness to calculate the force of contraction needed for their displacement. Pillars, wires, force-transducers or 2D-tissue strips are all used[26,56,57]. Recently, MPS of the heart that simultaneously measure contractile force and extracellular field potential have been described. Cardiomyocytes were cultured on a flexible electronic parylene-SR film with integrated gold-electrodes; contraction deflected the thin, flexible film and this generated compressive strain which was transmitted to allow direct, real-time monitoring of the excitation-contraction coupling[58]. The maximum force measured *in vivo* and *in vitro* depends on the tissue cross-section. Tissue force is thus best normalized to cross-sectional area, in principle enabling *in vitro* and *in vivo* comparisons. Nonetheless, measuring force as a function of the displacement of anchoring points as in EHTs is still prone to variability caused by differences in height of the tissue suspension points, insufficient information on the mechanical properties of anchoring points and differences in cross-sectional areas. Therefore, anchoring the tissue to a calibrated force-transducer still gives the best comparison with adult myocardium. The highest force values reported to date for MPS of the heart containing hiPSC-derived cardiomyocytes is 6.2 ± 0.8 mN/mm^2, achieved using standing pillars with serum-free medium[23]. This is similar to human infant myocardial force but still lower than adult heart *in vivo* (Supplementary Table 1). In addition to the maximum contraction force, dynamics in the contraction transient (e.g. contraction time, relaxation time) provide insight into the drug mechanism of action and report expected effect *in vivo*. For

example, the myosin activator omecamtiv mecarbil has been shown to increase both force of contraction and contraction time in hiPSC-derived cardiomyocyte EHTs[59], predicting the positive inotropic response in patients. A large study across multiple platforms showed that hiPSC-derived cardiomyocytes cultured in 2D and 3D are high predictive when based on output parameters such as time to peak, relaxation- and contraction time[54].

Adult human myocardial muscle strips show increased force at higher beating frequencies i.e. a positive FFR. This is not the case in mouse, failing or fetal hearts[27]. EHTs show positive FFR values after metabolic or electrical conditioning[23,25]. Relatively high baseline frequencies of spontaneously beating EHTs can mask the FFR. For this reason, ivabradine, a 'funny current' inhibitor, has been used to reduce the spontaneous beat-rate of EHTs to reveal a positive FFR, which could increase to about 200% of the baseline force. Ultimately, force is needed *in vivo* to generate enough pressure to circulate the blood through the body which is a highly relevant clinical read-out. Several different HoC systems have been designed to generate such pressure by engineering chambers and measured this pressure to assess the physiological relevance of their system. A HoC modelling ventricular chambers was used to perform pressure-volume loop measurements in a bioreactor and determined a maximum pressure of 50 μmHg[29], still far from the 120 mmHg *in vivo*[30]. While measuring output pressure is easier to compare with clinical values than force of contraction, the models require more complex engineering and typically higher cell numbers.

Digestion and absorption

The main function of the small intestine is to digest and absorb nutrients as source of energy for the body. The architecture of the epithelial barrier of the small intestine sustains this function through villi and microvilli, which greatly increase the surface area for nutrient breakdown and absorption into the bloodstream. The enterocytes, which form the main cell type of the small intestinal epithelial barrier, produce digestive- and drug metabolizing enzymes to enhance the bioavailability of food and drugs after oral intake.

In GoC devices, the epithelial cells can self-organize into 3D villus-like folds when exposed to continuous flow in the top and bottom channel. Computational 3D surface reconstruction based on microscopic Z-stack images showed a 2-fold increase in epithelial surface area within two days of seeding Caco-2 cells in the upper microchannel of a GoC system[31]. Increasing the microchannel height above 150 μm might have allowed the villi to grow closer to the ~700 μm described for human intestine and achieve the same 4.5-8.6 surface area enlargement (Supplementary Table 1). The surface area is further enlarged by the presence of microvilli on the surface of enterocytes, quantified to range from ˜15/μm^2 in the crypts to ˜200/μm^2 on the villus tips in human intestinal biopsies. Microvilli are often shown on enterocytes in GoCs but are rarely quantified. Exceptionally, one GoC study did quantify the microvilli density on the apical surface of primary duodenal tissue using electron microscopy and found upon dynamic force ˜7 microvilli per μm^2 [34]. This finding underlines the importance of quantification to further improve GoC systems and increase their physiological relevance.

Nutrient absorption by intestinal epithelial cells can be relatively easily measured in GoC systems. A GoC investigated glucose uptake rates by the intestinal epithelial barrier by perfusing glucose-containing medium through the apical channel and glucose-free medium through the basal channel, then quantifying the glucose concentrations at the channel outlets and the total number of epithelial cells in the system[31] (Supplementary Table 1). Multiple GoC studies have measured the activity of digestive enzymes such as sucrase-isomaltase[39] and aminopeptidase[37,38]. Both aminopeptidase studies confirmed increased enzyme activity upon fluid flow, however the kinetics are difficult to correlate with *in vivo* measurements of enzyme activity, as these mainly quantify substrates or metabolites in the systemic bloodstream after processing by multiple organs. In contrast, *in vitro* studies usually investigate the conversion rate of a substrate into a metabolite in a specific tissue or step of metabolism. The same issue arises when quantifying drug metabolizing enzyme activity. In very few cases, *in vivo* enzyme kinetics are described for a tissue specifically and can be compared directly to *in vitro* values. In a GoC system containing primary duodenal tissue for example, CYP3A4 enzymes transformed testosterone to 6β-hydroxytestosterone (6β-OH-T) with a metabolic rate of 0.056 nmol/min/mg protein which is lower than *in vivo* testosterone hydroxylation levels in human jejunum[34,40] (Supplementary Table 1). In contrast, other GoC studies used non-physiological substrates that are metabolized to fluorescent derivatives, which are not comparable with *in vivo* measurements. This illustrates the need for sets of validated reference compounds, for which the effects in the human body are well described. More complex GoC systems, linked to other organs, and *in silico* modeling may address this in the future and eventually allow relevant quantification of a more complete digestion and drug metabolism process.

Supplementary Discussion 5 | General designed features

Two designed features relevant for any *in vitro* model are the cell source and cell culture medium used. These features largely influence the emergent features.

Cell source

The most commonly used cell sources are primary human cells (either commercially available or patient-derived) or immortal(ized) or cancer cell lines since they are generally easy-to-use. All three are inexpensive and can show features of their tissue or organ source[60]. More recently, advances in stem cell biology enabled increasing application of either adult human stem cells (most easily derived from endodermal organs) or human induced pluripotent stem cells (hiPSCs) which are derived by reprogramming somatic cells to a state from which they can form derivatives of all organs[61]. hiPSC lines can be generated from healthy individuals or patients with genetic disorders and can be genetically engineered to introduce- or remove disease-specific mutations or variants for disease modelling[60]. They can also be geneticlally modified to incorporate cell type-specific (fluorescent) reporter constructs or phenotypic sensors. Drawbacks include cost, operator skill and an often immature phenotype although the latter can for some cells be obviated by inclusion in the MPS.

Media composition

MPS provide complex culture systems often with the inclusion of multiple tissue cell types from any of the sources above. Maintaining tissue-specific cell types requires the correct combination of nutrients, metabolites and growth factors. Blood vessels would normally be exposed to blood; cells in organs are generally either exposed to interstitial fluid or components of blood that have passed through the blood vessel wall. However, most current MPS have limited compatibility with physiological perfusates, such as whole blood, and there is to date no universal medium that can serve as a 'blood mimetic'[62]. Current MPS usually address this by either mixing media with different compositions that support the individual cell types in the system and examining the outcome empirically, or by compartmentalizing the device to 'feed' different cell types independently.

Supplementary Discussion 6 | Standardization and open platforms

Accurate comparisons of different MPS have become increasingly challenging as MPS use has grown and customized MPS designs have emerged. To achieve system-to-system and lab-to-lab comparability, standardization is required at multiple levels. Among these, agreement on methods for quantification of designed and emergent features in MPS is crucial to develop measurable standards applicable to (customized or commercial) MPS designs and platforms. This includes standardization of sensitivity and accuracy of the methods, reporting of data, and the use of reference compounds or methods that have been well-established *in vivo*. Developing MPS that can achieve measurable standards might require additional consensus on the materials and cells used, interfacing with existing lab infrastructure and various MPS, and operating strategies[63]. One approach that facilitates standardization is using MPS platforms with standardized interface that can accommodate and interconnect different types of MPS[64]. MPS platforms could incorporate the multiplicity of existing MPS within the uniformity of a familiar and standardized interface. Commercial platforms already partly offer this type of standardization. Other initiatives, such as the Translational Organ-on-Chip Platform (TOP)[65] and the Moore4Medical's Smart Multi-Well Plate[66], implement standardized constraints for chip geometry and interfaces[67], and may provide more generally applicable open technology platforms in which new MPS designs can be implemented interchangeably in 'plug-and-play' formats. These open technology platforms will enable the modular integration of sensors or use of existing laboratory equipment to generate quantitative read-outs of emergent features in MPS without having to develop tailored solutions for individual MPS platforms. It has been argued that, by embedding a variety of MPS with a uniform and standardized interface, MPS platforms could contribute to establishing more reproducible and lab-independent MPS practice, amenable to wider adoption by end users and regulatory acceptance. To facilitate this, MPS developers should inform the design of their devices with the standards for geometry and interfaces adopted in the MPS platforms, in a process that gradually converges towards eliciting a set of shared templates for MPS design. In this way, these platforms will aid in standardizing the design and operation of MPS and pave the way to multi-organ systems.

Supplementary references

1. Offeddu, G. S. *et al.* Application of Transmural Flow Across In Vitro Microvasculature Enables Direct Sampling of Interstitial Therapeutic Molecule Distribution. *Microcirculation-on-Chip* **15**, e1902393 (2019).
2. Swartz, M. A. & Fleury, M. E. Interstitial flow and its effects in soft tissues. *Annu. Rev. Biomed. Eng.* **9**, 229–256 (2007).
3. Jalili-firoozinezhad, S. *et al.* A complex human gut microbiome cultured in an anaerobic intestine-on-a-chip. *Nat. Biomed. Eng.* **3**, 520–531 (2019).
4. Villmones, H. C. *et al.* Species Level Description of the Human Ileal Bacterial Microbiota. *Sci. Rep.* **8**, (2018).
5. Collison, J. L., Carlin, L. M., Eichmann, M., Geissmann, F. & Peakman, M. Heterogeneity in the Locomotory Behavior of Human Monocyte Subsets over Human Vascular Endothelium In Vitro. *J. Immunol.* **195**, 1162–1170 (2015).
6. Buscher, K., Marcovecchio, P., Hedrick, C. C. & Ley, K. Patrolling Mechanics of Non-Classical Monocytes in Vascular Inflammation. *Front. Cardiovasc. Med.* **4**, (2017).
7. Maurer, M. *et al.* A three-dimensional immunocompetent intestine-on-chip model as in vitro platform for functional and microbial interaction studies. *Biomaterials* **220**, 119396 (2019).
8. Hayat, M., Cairns, A., Dixon, M. F. & O'Mahony, S. Quantitation of intraepithelial lymphocytes in human duodenum: what is normal? *J. Clin. Pathol.* **55**, 393–395 (2002).
9. Sontheimer-Phelps, A. *et al.* Human Colon-on-a-Chip Enables Continuous In Vitro Analysis of Colon Mucus Layer Accumulation and Physiology. *Cell Mol Gastroenterol Hepatol.* **9**, 507–526 (2020).
10. Dutton, J. S., Hinman, S. S., Kim, R., Wang, Y. & Allbritton, N. L. Primary Cell-Derived Intestinal Models: Recapitulating Physiology. *Trends Biotechnol.* **37**, 744–760 (2019).
11. Spijkers, X. M. *et al.* A directional 3D neurite outgrowth model for studying motor axon biology and disease. *Sci. Rep.* **11**, 2080 (2021).
12. Stifani, N. Motor neurons and the generation of spinal motor neuron diversity. *Front. Cell. Neurosci.* **8**, 293 (2014).
13. Sharma, A. D. *et al.* Engineering a 3D functional human peripheral nerve in vitro using the Nerve-on-a-Chip platform. *Sci. Rep.* **9**, 8921 (2019).
14. Cercignani, M. *et al.* Characterizing axonal myelination within the healthy population: a tract-by-tract mapping of effects of age and gender on the fiber g-ratio. *Neurobiol. Aging* **49**, 109–118 (2017).
15. Espinosa-Hoyos, D. *et al.* Engineered 3D-printed artificial axons. *Sci. Rep.* **8**, 478 (2018).
16. Tomassy, G. S. *et al.* Distinct Profiles of Myelin Distribution Along Single Axons of Pyramidal Neurons in the Neocortex. *Science (80-.).* **344**, 319–324 (2014).
17. Lu, X., Kim-Han, J. S., O'Malley, K. L. & Sakiyama-Elbert, S. E. A microdevice platform for visualizing mitochondrial transport in aligned dopaminergic axons. *J. Neurosci. Methods* **209**, 35–39 (2012).
18. Takihara, Y. *et al.* In vivo imaging of axonal transport of mitochondria in the diseased and aged mammalian CNS. *Proc. Natl. Acad. Sci. U. S. A.* **112**, 10515–10520 (2015).
19. Mathur, A. *et al.* Human iPSC-based cardiac microphysiological system for drug screening applications. *Sci. Rep.* **5**, 8883 (2015).
20. Drouin, E., Charpentier, F., Gauthier, C., Laurent, K. & Le Marec, H. Electrophysiologic characteristics of cells spanning the left ventricular wall of human heart: Evidence for presence of M cells. *J. Am. Coll. Cardiol.* **26**, 185–192 (1995).
21. Tulloch, N. L. *et al.* Growth of engineered human myocardium with mechanical loading and vascular coculture. *Circ. Res.* **109**, 47–59 (2011).
22. Mills, R. J. *et al.* Functional screening in human cardiac organoids reveals a metabolic mechanism for cardiomyocyte cell cycle arrest. *Proc. Natl. Acad. Sci.* **114**, E8372–E8381 (2017).
23. Tiburcy, M. *et al.* Defined engineered human myocardium with advanced maturation for applications in heart failure modeling and repair. *Circulation* **135**, 1832–1847 (2017).
24. Hasenfuss, G. *et al.* Energetics of isometric force development in control and volume-overload human myocardium. Comparison with animal species. *Circ. Res.* **68**, 836–846 (1991).
25. Zhao, Y. *et al.* Towards chamber specific heart-on-a-chip for drug testing applications. *Adv. Drug Deliv. Rev.* **165–166**, 60–76 (2020).
26. Ronaldson-Bouchard, K. *et al.* Advanced maturation of human cardiac tissue grown from pluripotent stem cells. *Nature* **556**, 239–243 (2018).
27. Wiegerinck, R. F. *et al.* Force frequency relationship of the human ventricle increases during early postnatal development. *Pediatr. Res.* **65**, 414–419 (2009).
28. Gerdes, A. M. *et al.* Structural remodeling of cardiac myocytes in patients with ischemic cardiomyopathy. *Circulation* **86**, 426–430 (1992).

29. MacQueen, L. A. *et al.* A tissue-engineered scale model of the heart ventricle. *Nat. Biomed. Eng.* **2**, 930–941 (2018).
30. Timmis, A. *et al.* European society of cardiology: Cardiovascular disease statistics 2019. *Eur. Heart J.* **41**, 12–85 (2020).
31. Kim, H. & Ingber, D. Gut-on-a-Chip microenvironment induces human intestinal cells to undergo villus differentiation. *Integr. Biol.* **5**, 1130–1140 (2013).
32. Helander, K. G., Åhren, C., Philipson, B. M., Samuelsson, B. M. & Ójerskog, B. Structure of mucosa in continent ileal reservoirs 15 to 19 years after construction. *Hum. Pathol.* **21**, 1235–1238 (1990).
33. Helander, H. F. & Fändriks, L. Surface area of the digestive tract-revisited. *Scand. J. Gastroenterol.* **49**, 681–689 (2014).
34. Kasendra, M. *et al.* Duodenum intestine-chip for preclinical drug assessment in a human relevant model. *Elife* **9**, e50135 (2020).
35. Brown, A. L. Microvilli of the human jejunal epithelial cell. *J Cell Biol.* **12**, 623–627 (1962).
36. Gray, G. M. & Ingelfinger, F. J. Intestinal absorption of sucrose in man: interrelation of hydrolysis and monosaccharide product absorption. *J. Clin. Invest.* **45**, 388–398 (1966).
37. Kim, H., Huh, D., Hamilton, G. & Ingber, D. Human gut-on-a-chip inhabited by microbial flora that experiences intestinal peristalsis-like motions and flow. *Lab Chip* **12**, 2165–2174 (2012).
38. Shim, K. Y. *et al.* Microfluidic gut-on-a-chip with three-dimensional villi structure. *Biomed. Microdevices* **19**, 37 (2017).
39. Kasendra, M. *et al.* Development of a primary human Small Intestine-on-a-Chip using biopsy-derived organoids. *Sci. Rep.* **8**, 2871 (2018).
40. Obach, R. S., Zhang, Q. Y., Dunbar, D. & Kaminsky, L. S. Metabolic characterization of the major human small intestinal cytochrome P450S. *Drug Metab. Dispos.* **29**, 347–352 (2001).
41. Lun, M. P., Monuki, E. S. & Lehtinen, M. K. Development and functions of the choroid plexus-cerebrospinal fluid system. *Nat. Rev. Neurosci.* **16**, 445–457 (2015).
42. Park, J. *et al.* Three-dimensional brain-on-a-chip with an interstitial level of flow and its application as an in vitro model of Alzheimer's disease. *Lab Chip* **15**, 141–150 (2015).
43. Scepanovic, P. *et al.* A comprehensive assessment of demographic, environmental, and host genetic associations with gut microbiome diversity in healthy individuals. *Microbiome* **7**, 130 (2019).
44. Fajgenbaum, D. C. & June, C. H. Cytokine Storm. *N. Engl. J. Med.* **383**, 2255–2273 (2020).
45. Woodfin, A. *et al.* The junctional adhesion molecule JAM-C regulates polarized transendothelial migration of neutrophils in vivo. *Nat. Immunol.* **12**, 761–769 (2011).
46. Proebstl, D. *et al.* Pericytes support neutrophil subendothelial cell crawling and breaching of venular walls in vivo. *J. Exp. Med.* **209**, 1219–1234 (2012).
47. McMinn, P. H., Hind, L. E., Huttenlocher, A. & Beebe, D. J. Neutrophil trafficking on-a-chip: an in vitro, organotypic model for investigating neutrophil priming, extravasation, and migration with spatiotemporal control. *Lab Chip* **19**, 3697–3705 (2019).
48. Boussommier-Calleja, A. *et al.* The effects of monocytes on tumor cell extravasation in a 3D vascularized microfluidic model. *Biomaterials* **198**, 180–193 (2019).
49. Pérez-Rodríguez, S., Huang, S. A., Borau, C., García-Aznar, J. M. & Polacheck, W. J. Microfluidic model of monocyte extravasation reveals the role of hemodynamics and subendothelial matrix mechanics in regulating endothelial integrity. *Biomicrofluidics* **15**, 054102 (2021).
50. Bray, M. A., Sheehy, S. P. & Parker, K. K. Sarcomere alignment is regulated by myocyte shape. *Cell Motil. Cytoskeleton* **65**, 641–651 (2008).
51. Ribeiro, M. C. *et al.* Functional maturation of human pluripotent stem cell derived cardiomyocytes invitro - Correlation between contraction force and electrophysiology. *Biomaterials* **51**, 138–150 (2015).
52. Ariyasinghe, N. R., Lyra-Leite, D. M. & McCain, M. L. Engineering cardiac microphysiological systems to model pathological extracellular matrix remodeling. *Am. J. Physiol. Circ. Physiol.* **315**, H771–H789 (2018).
53. Salick, M. R. *et al.* Micropattern width dependent sarcomere development in human ESC-derived cardiomyocytes. *Biomaterials* **35**, 4454–4464 (2014).
54. Saleem, U. *et al.* Blinded, Multicenter Evaluation of Drug-induced Changes in Contractility Using Human-induced Pluripotent Stem Cell-derived Cardiomyocytes. *Toxicol. Sci.* **176**, 103–123 (2020).
55. Marsano, A. *et al.* Beating heart on a chip: a novel microfluidic platform to generate functional 3D cardiac microtissues. *Lab Chip* **16**, 599–610 (2016).
56. Wijnker, P. J. M. *et al.* Comparison of the effects of a truncating and a missense MYBPC3 mutation on contractile parameters of engineered heart tissue. *J. Mol. Cell. Cardiol.* **97**, 82–92 (2016).
57. Grosberg, A., Alford, P. W., McCain, M. L. & Parker, K. K. Ensembles of engineered cardiac tissues for physiological and pharmacological study: Heart on a chip. *Lab Chip* **11**, 4165–4173 (2011).

58. Ohya, T. *et al.* Simultaneous measurement of contractile force and field potential of dynamically beating human iPS cell-derived cardiac cell sheet-tissue with flexible electronics. *Lab Chip* **21**, 3899–3909 (2021).
59. Saleem, U. *et al.* Force and Calcium Transients Analysis in Human Engineered Heart Tissues Reveals Positive Force-Frequency Relation at Physiological Frequency. *Stem Cell Reports* **14**, 312–324 (2020).
60. Van Den Berg, A., Mummery, C. L., Passier, R. & Van der Meer, A. D. Personalised organs-on-chips: functional testing for precision medicine. *Lab Chip* **19**, 198–205 (2019).
61. Sharma, A., Sances, S., Workman, M. J. & Svendsen, C. N. Multi-lineage Human iPSC-Derived Platforms for Disease Modeling and Drug Discovery. *Cell Stem Cell* **26**, 309–329 (2020).
62. Low, L. A., Mummery, C. L., Berridge, B. R., Austin, C. P. & Tagle, D. A. Organs-on-chips: into the next decade. *Nat. Rev. Drug Discov.* **20**, 345–361 (2020).
63. Piergiovanni, M., Leite, S. B., Corvi, R. & Whelan, M. Standardisation needs for organ on chip devices. *Lab Chip* **21**, 2857–2868 (2021).
64. Mastrangeli, M. *et al.* Building blocks for a European organ-on-chip roadmap. *ALTEX* **36**, 481–492 (2019).
65. Vollertsen, A. R. *et al.* Facilitating implementation of organs-on-chips by open platform technology. *Biomicrofluidics* **15**, 051301 (2021).
66. Mastrangeli, M. *et al.* Microelectromechanical Organs-on-Chip. *21st Int. Conf. Solid-State Sensors, Actuators Microsystems, TRANSDUCERS 2021* 102–107 (2021). doi:10.1109/Transducers50396.2021.9495646
67. ISO 22916: 2022. Microfluidic devices — Interoperability requirements for dimensions, connections and initial device classification. Available at: https://www.iso.org/standard/74157.html.